BIOCHEMISTRY
including biophysical chemistry & molecular biology

Article

pubs.acs.org/biochemistry

Probing the Conformational Flexibility of Monomeric FtsZ in GTP-Bound, GDP-Bound, and Nucleotide-Free States

Kathiresan Natarajan and Sanjib Senapati*

Department of Biotechnology, Indian Institute of Technology Madras, Chennai 600036, India

Supporting Information

ABSTRACT: The mechanism of nucleotide-regulated assembly and disassembly of the prokaryotic cell division protein FtsZ is not yet clearly understood. In this work, we attempt to characterize the functional motions in monomeric FtsZ through molecular dynamics simulations and essential dynamics (ED) analyses and correlate those motions to FtsZ assembly and disassembly. Results suggest that the nucleotide binding subdomain of FtsZ can switch between multitudes of curved conformations in all nucleotide states, but it prefers to be in an assembly competent less curved conformation in the GTP-bound state. Further, the GDP to GTP exchange invokes a subtle conformational change in the nucleotide binding pocket that tends to align the top portion of core helix H7 along the longitudinal axis of the protein. ED analyses suggest that the longitudinal movements of H7 and the adjacent H6−H7 region modulate the motions of C-domain elements coherently. These longitudinal movements of functionally relevant H7, H6−H7, T3, T7, and H10 regions are likely to facilitate the assembly of GTP-FtsZ into straight filament. On the other hand, the observed radial or random movements of FtsZ residues in the GDP state might not allow the monomers to assemble as efficiently as GTP-bound monomers and could produce curved filaments. Our results correlate very well with recent mutagenesis data that inferred FtsZ conformational flexibility and the involvement of the H6−H7 region in assembly.

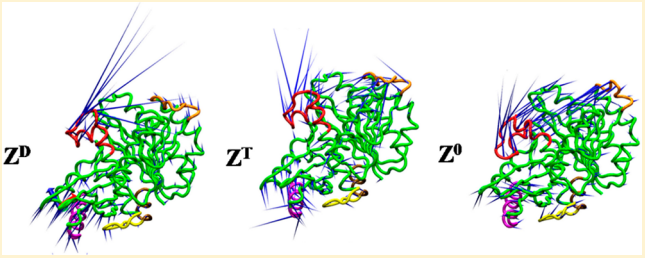

FtsZ (Filamentous temperature sensitive protein Z) is a bacterial GTPase that is structurally similar to eukaryotic cytoskeletal protein tubulin.[1] It plays pivotal roles in bacterial cytokinesis by forming a dynamic ring around the midcell to define the division plane.[2−4] The nearly universal distribution of FtsZ in bacteria and its key role in cell division have made FtsZ an attractive target for designing new antibiotics.[5−8] The recent successful synthesis of an effective FtsZ inhibitor[9] against multidrug resistant *Staphylococcus aureus* has raised hopes about a new class of future antibiotics targeting FtsZ. This inhibitor suppresses bacterial cell division by inducing FtsZ filament assembly and condensation.[10,11] By contrast, several C8-substituted GTP analogues[12−14] and small molecules[15−20] arrest cell division by inhibiting the FtsZ assembly dynamics. Thus, FtsZ assembly dynamics has received much attention recently.

Assembly dynamics of FtsZ is primarily regulated by the bound nucleotide. The protein requires GTP to assemble but disassembles as a result of hydrolysis of GTP to GDP.[3] The filaments of FtsZ can be straight or curved depending on the nucleotide state. While GTP binding displaces the equilibrium to the straight filaments, GDP-bound FtsZ filaments that eventually depolymerize tend to be curved.[21] The peeled-away GDP-FtsZ monomers exchange GDP for GTP in solution and recycle into the polymers, similar to the process for tubulin.[21,22] It has long been hypothesized that GTP-bound FtsZ monomers favor a "straight" conformation suitable for filament assembly, while the GDP-FtsZ subunits favor a "curved" conformation that leads filament disassembly.[23] However, the recent crystal structures of *Methanococcus jannaschii* FtsZ (MjFtsZ) in GDP- and GTP-bound states [Protein Data Bank (PDB) entries 1FSZ and 1W5E, respectively] show no significant structural changes between the two forms,[24] but a significant root-mean-square deviation (rmsd) of 1.45 Å was observed between GDP-MjFtsZ and nucleotide-free MjFtsZ (PDB entry 1W59).

It is also suggested that FtsZ filaments can generate constriction force, necessary for dividing the cell, through iterative cycles of GTP hydrolysis.[25−28] It has been demonstrated in a recent experiment that FtsZ can assemble into rings even in the absence of other division proteins and is capable of generating the constriction force on the liposome wall.[27] Several theoretical models have also proposed GTP hydrolysis as a force-generating mechanism during bacterial cell division.[29−32] All these recent studies, thus, imply that the regulation of FtsZ assembly and disassembly and polymer dynamics is primarily determined by nucleotide states, where the GTP state facilitates filament assembly and the GDP state disassembly.

Because MjFtsZ crystal structures showed no significant structural differences between GDP- and GTP-bound states,

Received: February 11, 2013
Revised: April 18, 2013
Published: April 25, 2013

dx.doi.org/10.1021/bi400170f | *Biochemistry* 2013, 52, 3543−3551

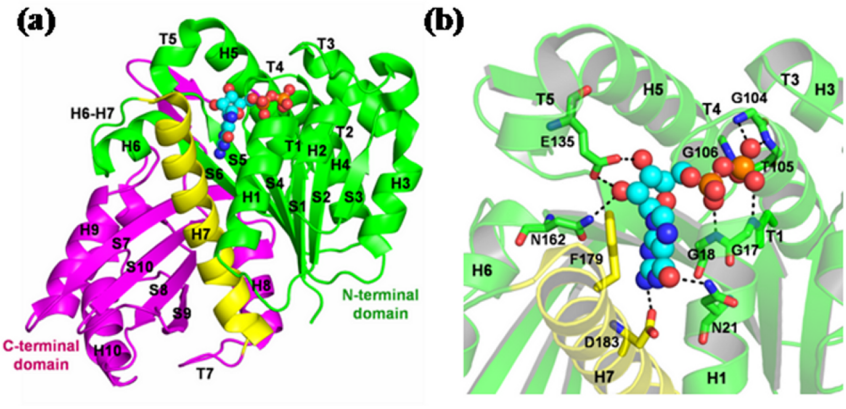

Figure 1. (a) Crystal structure of AaFtsZ bound to GDP. The N- and C-terminal domains are colored green and pink, respectively. Also shown is the core helix H7 (yellow). (b) Detailed view of the nucleotide binding site and GDP interactions. The interacting protein residues are shown as licorice, and GDP is shown in ball-and-stick mode.

the interesting question of how different curvatures originate during FtsZ assembly and disassembly even though FtsZ subunits are not affected by nucleotide state arises. To understand this phenomenon in detail, we have taken the crystal structure of GDP-FtsZ from *Aquifex aeolicus* (AaFtsZ), the best resolution model available till date (resolution of 1.7 Å),[24] and generated the structural conformations of GTP-FtsZ and nucleotide-free FtsZ by performing extensive all-atom molecular dynamics (MD) simulations up to 200 ns. Subsequently, a comparative study of the trajectories was conducted by essential dynamics (ED) analysis. A similar strategy, applied to correlate the nucleotide-dependent conformational changes and effects of mutations on tubulin assembly, has shown promise in explaining the experimental observations very accurately.[33,34] The results of our study suggest that the GDP- and GTP-bound FtsZ are structurally similar, even though they differ substantially in their dynamics. The H6−H7 region, in particular, shows significantly different flexibility, which can modulate the FtsZ assembly process by attaining a wide range of conformations. This mainly stems from the individual interactions of GDP and GTP with the FtsZ binding cleft, which differed substantially along the simulation trajectories as quantified by percent occurrences of H-bonds and polar interactions, though they appear to be similar in the average structures.

METHODS

Molecular Dynamics Simulations. Figure 1a presents the crystal structure of AaFtsZ bound to GDP (PDB entry 2R6R[24]). It consists of two globular domains, an N-terminal nucleotide binding domain and a C-terminal domain. Two domains are connected via core helix H7 and loop T7. During filament formation, the C-terminal domain from the upper subunit contacts the N-domain from the lower subunit.[22] The secondary structural elements that are reported to be involved in filament formation include helix H7, loop T3, and the H6−H7 region from the N-domain and helices H8 and H10 and loop T7 from the C-domain. Figure 1b shows a detailed view of the nucleotide binding site and GDP interactions.

We performed three independent all-atom MD simulations of FtsZ bound to GDP (Z^D state), bound to GTP (Z^T state), and free of nucleotides (Z^0 state). The simulation of the Z^D state was initiated from the crystal structure of GDP-bound FtsZ (PDB entry 2R6R[24]). The hydrogens for heavy atoms were added to this structure by the leap program of Amber version 11.0.[35] Added hydrogens were energy minimized for 2000 steps using the steepest descent algorithm. The protonation states of histidines, HID or HIE, were determined by the local hydrogen bonding network using WHATIF.[36] A set of partial atomic charges for GDP (and later for GTP) was obtained via quantum electronic structure calculations. Using Gaussian 09[37] with the 6-31+G* basis set, we performed a Hartree−Fock geometry optimization procedure. The atom-centered RESP charges[38] were determined via fits to the electrostatic potentials obtained from the calculated wave functions. The missing interaction parameters in the nucleotides were generated using antechamber tools in Amber.

After the added atoms in the gas phase had been relaxed, the structure was solvated in an octahedral periodic box of explicit water with water molecules extending 12 Å outside the protein on all sides. The three-site TIP3P model[39] was chosen to describe the water molecules, and simulations were conducted with an ionic strength of 150 mM KCl. A particle-mesh Ewald sum[40] with a 10 Å cutoff was used to treat the long-range electrostatics. SHAKE[41] was used to constrain bond lengths between heavy atoms and hydrogens. The system was equilibrated for 20 ns with a simulation time step of 2 fs to obtain a model structure for GDP-FtsZ. During this period, the energy components, mass density, and rmsds were seen to be converging. This equilibrated structure was further engineered to generate the starting structure for the simulations of Z^T and Z^0 states. A γ-phosphate and Mg^{2+} ion were introduced into the equilibrated structure of the Z^D simulation to obtain a crude initial structure of the Z^T state, whereas the structure of the Z^0 state was obtained by removing the nucleotide. The initial Z^T and Z^0 structures were then equilibrated via a 20 ns MD run to obtain the model structures for GTP-FtsZ and nucleotide-free FtsZ. All three model structures for Z^D, Z^T, and Z^0 were further simulated to generate 200 ns MD data, upon which all analyses were performed. The data were saved at an interval of 2 ps for analyses. All simulations were performed using NAMD version 2.7[42] with the AMBERFF99SB force field[43] on 64 processors of an Infiniband Xeon E5472 linux cluster. It is worth mentioning that here we employ an isobaric−isothermal rather than canonical ensemble with the aim of reproducing the *in vitro* effects of the nucleotide on FtsZ assembly. *In vivo*, the FtsZ assembly process is more complex and regulated by nucleotides and various associated proteins.[2,3]

dx.doi.org/10.1021/bi400170f | *Biochemistry* 2013, 52, 3543−3551

Essential Dynamics Analysis. Essential dynamics (ED) analysis, also termed principal component analysis (PCA), is utilized here to study the large concerted motions. PCA can transform the original space of correlated variables into a reduced space of independent variables (the principal components).[44] In other words, PCA transforms the original high-dimensional representation of protein motions into a low-dimensional one that captures the dominant modes of the protein motions. The analysis involves two main steps: (i) calculation of the covariance matrix, **C**, of the positional deviations and (ii) diagnolization of this matrix. The 3*N*-dimensional covariance is calculated on the basis of an ensemble of protein structures, whose elements are defined as

$$C_{ij} = \langle (x_i - \langle x_i \rangle)(x_j - \langle x_j \rangle) \rangle$$

where x_i and x_j are the atomic coordinates and broken brackets denote the ensemble average. The diagonalization of the symmetric matrix **C** is equivalent to solving the eigenvalue problem:

$$\mathbf{A}^{\mathbf{T}} \cdot \mathbf{C} \cdot \mathbf{A} = \lambda$$

where **A** represents the eigenvectors and λ represents the associated eigenvalues. In a sense, the eigenvectors are directions in configurational space that represent collective motions. Corresponding eigenvalues define the mean-square fluctuation of the motion along these vectors.

The collective variables are ranked according to their contribution to the total mean-square fluctuation.[44] Prior to the calculation of the covariance matrix, we removed the overall rotation and translation.

The essential dynamics analysis was conducted using the GROMACS suite of programs.[45] The porcupine plots were generated using DYNATRAJ.[46] These plots provide a graphical representation of the motion held in eigenvector v_i. To visualize the motion, a cone is drawn for each residue corresponding to the direction of its movement. The porcupine plots were visualized using VMD.[47]

RESULTS

Structural Behavior of FtsZ in Z^D, Z^T, and, Z^0 States. We have performed three independent all-atom MD simulations of FtsZ, liganded to GDP (Z^D), liganded to GTP (Z^T), and free of ligands (Z^0). To investigate the effects of nucleotide state on FtsZ structure, we have calculated rmsds of the simulated structures relative to the crystal conformation. As Figure 2a shows, the Z^D and Z^T states do not show a significant deviation from the crystal conformation. The time evolutions of the rmsds of these two states are very similar, suggesting that the FtsZ protein in GDP- and GTP-bound forms is structurally indifferent. The superposition of the time-averaged structures, shown in Figure 2b, indeed shows such a similarity with a Δrmsd of only ~0.7 Å. This finding matches favorably well with the crystal structures of MjFtsZ, where the FtsZ subunits from this species have shown no significant structural changes between the GDP- and GTP-bound forms.[24] The average structures were obtained by superposing the protein conformations onto that in the starting structure and taking the mean of the atom positions at every 25 ps interval during the last 50 ns run.

The comparison of nucleotide-bound and nucleotide-free FtsZ structures, however, shows many differences. The average rmsd of the Z^0 state from the simulated GDP-bound FtsZ

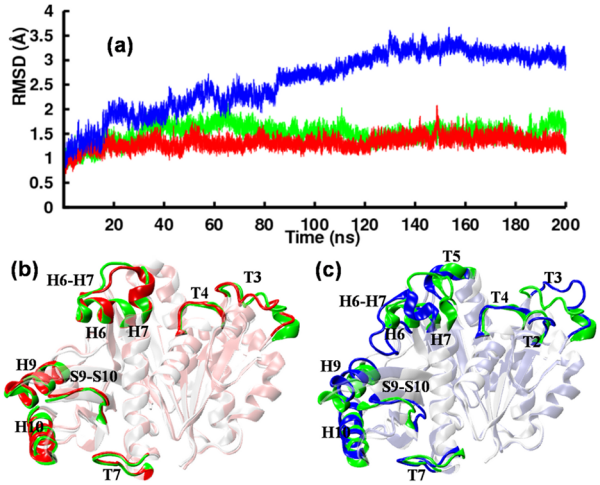

Figure 2. Nucleotide-dependent structural changes in FtsZ. (a) Cα rmsds of simulated FtsZ structures from the crystal conformation as a function of time. The rmsds were calculated by superposing each snapshot on the starting structure to remove the rigid body translations and rotations. Color scheme: green for Z^D, red for Z^T, and blue for Z^0. (b) Superposition of the time-averaged structures of the Z^D (green) and Z^T (red) states. (c) Superposition of time-averaged structures of the Z^D (green) and Z^0 (blue) states. Secondary structural elements that underwent the most significant conformational changes are highlighted. A slight rotation of the C-terminal domain in the Z^0 state was observed.

structure was 1.72 Å during the final 50 ns simulation run, and the majority of functionally relevant loops and helices attained different conformations. This is shown in Figure 2c, where loops T2, T3, T4, and T5, the H6−H7 region, and helices H6 and H7 in the N-domain and loops T7 and S9−S10 and helices H9 and H10 in C-domain are highlighted for Z^D and Z^0 states. Loops T3, T5, and T7, helices H8 and H10, and the H6−H7 region are known to be involved in protofilament contacts.[22] In particular, loops T2 and T3 and the H6−H7 region have undergone significant conformational changes and opened up significantly. Very interestingly, the removal of the nucleotide has yielded a twisted bending in core helix H7 and a slight rotation in the C-terminal domain toward the N-domain. The domain shifting could be seen easily by superposing the N-terminal domain alone and comparing the C-domains in two states (Figure S1 of the Supporting Information). The twisted bending of helix H7 along with the C-domain movement has opened the nucleotide binding cleft in the Z^0 state, as shown in Figure S1 of the Supporting Information.

Dynamics of FtsZ in Z^D, Z^T, and, Z^0 States. Positional shifts of individual residues can be estimated from the residue-level rmsds, calculated through time-averaged rmsds with respect to the starting structure. The comparison in Figure 3a shows that the residues in Z^D and Z^T states behave differently in the H6−H7 and nucleotide binding regions. The H6−H7 region is composed of helix H6, loop H6−H7, and the top part of helix H7 (residues 160−180) and is known to be involved in longitudinal interactions during FtsZ assembly. The nucleotide binding region, particularly the T3 loop, also is involved in inter-FtsZ interactions along the longitudinal direction. The Z^0 state, as expected, shows large rmsds for a majority of the residues, particularly in loops T3 and T4, helices H3 and H9, and the region H6−H7. These large deviations can be attributed to the increased flexibility of the secondary structural elements in the absence of the nucleotide.

dx.doi.org/10.1021/bi400170f | *Biochemistry* 2013, 52, 3543−3551

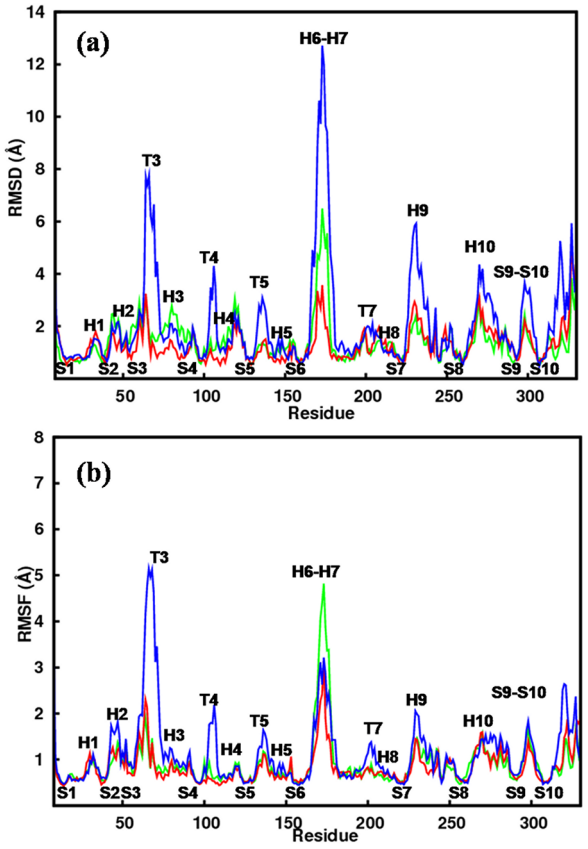

Figure 3. Residue-level displacements and fluctuations of FtsZ in three nucleotide states. (a) Positional shifts of individual residues during simulation. The color scheme is similar to that of Figure 2. (b) Root-mean-squared fluctuations [rmsf = $(\langle \Delta r^2 \rangle)^{1/2} = (3B/8\pi^2)^{1/2}$] of the C$\alpha$ atoms in three states of the FtsZ monomer. The regions with the most significant changes are labeled.

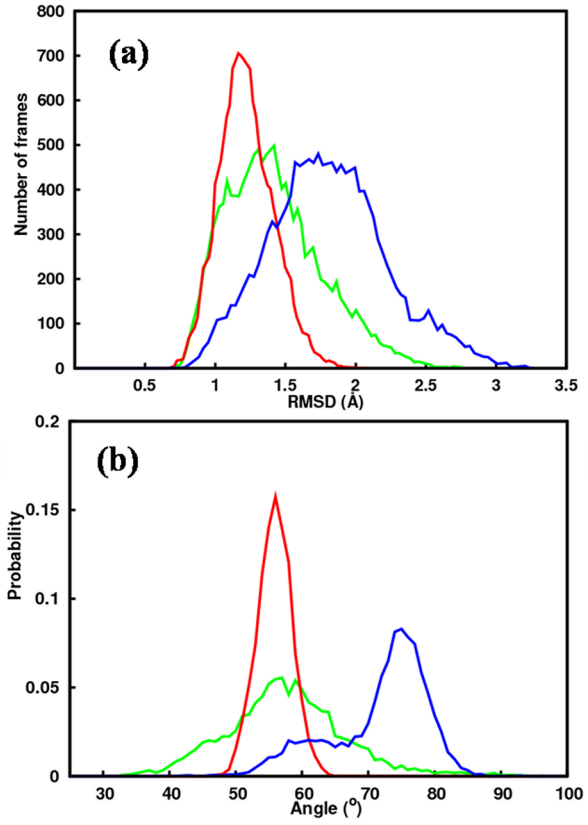

Figure 4. Conformational flexibility of FtsZ in three nucleotide states. (a) Distribution of the simulated FtsZ structures in different nucleotide states. Analysis was performed by clustering the structures based on their Cα rmsd values with respect to the starting configuration. The color scheme is similar to that of Figure 2. (b) Probability distribution of the angles between the top portion of core helix H7 and helix H1.

The flexibility of the residues was better distinguished via the root-mean-square fluctuations (rmsf) of the Cα atoms, along the entire trajectory. As Figure 3b indicates, Z^D and Z^T states show distinct differences in flexibility in the H6−H7 region. The nucleotide binding region also displays a small change in flexibility under the influence of the γ-phosphate. The T4 loop shows reduced flexibility in the GTP state. A minor change is also observed in loop T5. However, T3 is found to be similar in the GDP and GTP states. The nucleotide-free Z^0 state shows larger rmsfs in both N- and C-domains. The flexibility of loops T4 and T5 is more pronounced because of the absence of the nucleotide. The high flexibility of the H6−H7 region is also observed in the Z^0 state. Though this region became stable after simulation for 25 ns in this state, it continues to fluctuate for the entire simulation stretch in the Z^D state. This can be clearly seen from the time evolution of the local rmsd (Figure S2 of the Supporting Information). The calculated rmsfs could also trace the rigid subdomains in N- and C-terminal regions,[48] composed of sheets S1−S6 and S7−S10, respectively, which are less flexible because of the dense interaction network.

Figure 4a shows the rmsd distributions of all the sampled configurations during the 200 ns production phase. Most of the configurations in the Z^0 state had rmsds larger than those of the Z^D and Z^T states, further suggesting that FtsZ undergoes larger conformational changes in the absence of a nucleotide. A more detailed structural analysis showed differences in the movement of the core helix, H7. To characterize the movement of H7 further, we calculated the angle between H7 and helix H1 during the 200 ns simulation period (Figure 4b). We have selected this angle because a small displacement was noted between sections of H7 and H1 among the available FtsZ crystal structures.[24] Panels a and b of Figure 4 imply that the most probable conformations of FtsZ in Z^D and Z^T states are similar (the location of peaks at similar rmsds and angles). However, the Z^D state and also the Z^0 state are more flexible and can attain a multitude of conformations, e.g., moderately curved ($\angle$H7−H1 < 50°), curved [$\angle$H7−H1 = 50−65°; crystal structure values of 60° for GDP-FtsZ (PDB entry 2R6R)[24] and 57° for 8-morpholino-GTP-FtsZ (PDB entry 2R75[24])], and strongly curved ($\angle$H7−H1 > 65°). The Z^T state, on the other hand, appears to be more compact and prefers to remain in a less curved conformation, as characterized by its movement within a narrow rmsd range and a smaller H7−H1 angle. The results thus clearly demonstrate the conformational flexibility in FtsZ[48] and suggest that the role of GTP could be to keep FtsZ in an assembly competent less curved conformation. It is also likely that the modular flexibility of the H6−H7 region arising due to the change in nucleotide state could help in generating the constriction force essential for FtsZ function in cell division. Our results are consistent with a recent simulation study in which GTP- and GDP-bound FtsZ dimers were shown to have inherently different conformational flexibility.[49]

Nucleotide Interactions in FtsZ. The individual interactions of GDP and GTP in the FtsZ binding cleft were also

dx.doi.org/10.1021/bi400170f | *Biochemistry* 2013, 52, 3543−3551

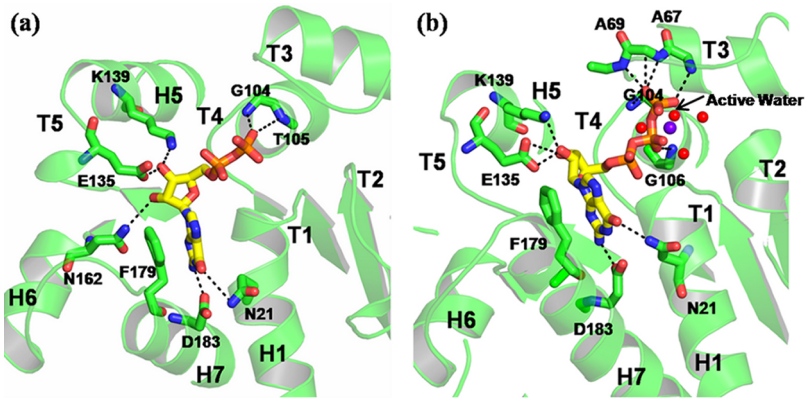

Figure 5. Mode of interaction of the nucleotides in (a) GDP-FtsZ and (b) GTP-FtsZ. The structures were obtained by averaging over the final 50 ns of data. The nucleotides are shown at the center, and the neighboring interacting protein residues are included. Dotted lines denote the H-bonding interactions. The location of the Mg^{2+} ion (purple sphere) and the adjoining water molecules (red spheres) are shown in GTP-FtsZ. The active water molecule is denoted with an arrow.

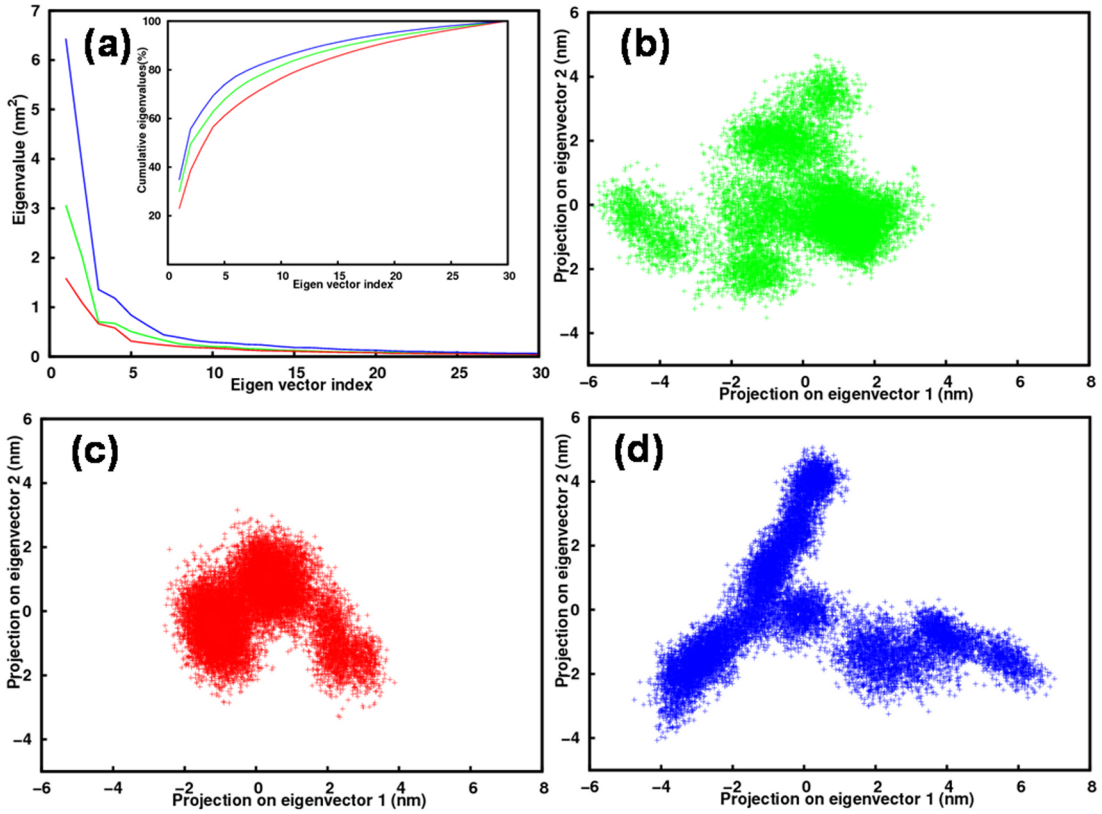

Figure 6. Eigenvalue profile and comparative sampling of essential motions in three nucleotide states of FtsZ. (a) Eigenvalues of the first 30 eigenvectors, derived from ED analyses of the simulation trajectories of the Z^D (green), Z^T (red), and Z^0 (blue) states. The inset shows the cumulative contribution of these eigenvectors. (b–d) Two-dimensional projections of simulation structures onto the plane constituted by the first two principal components: (b) Z^D state, (c) Z^T state, and (d) Z^0 state.

compared. Figure 5 shows the major interactions present in the average structures of the two states. Although the interactions appear to be similar in the average structures, their extent as quantified by percent occurrences along the simulation trajectories differed in the two states. For example, the nucleotide α-phosphate forms H-bonds with NH of G17 and NH of G18 in 99.68 and 97.74% of the total samples, respectively, in the Z^T state but in only 30.85 and 80.54% of the samples, respectively, in the Z^D state. The β-phosphate interacts with NH of G104 and NH of G105/NH of G106 of loop T4 in 99.82 and 96.22% of the total samples, respectively, in the Z^T state but in only 98.15 and 80.44% of the samples, respectively, in the Z^D state. The nucleotide ribose ring interacts with E135 of loop T5 in 98.56% of the samples in the Z^T state but in only 43.45% of the samples in the Z^D state. An interaction is considered to be present when the distance between the pair of atoms was <3.5 Å. The guanine ring of the nucleotide was found to be stacked between F179 from helix H7 and G18 from helix H1 in both Z^T and Z^D states. A more detailed structural inspection of the FtsZ crystal structures and molecular dynamics trajectories indicated that residue F179 plays a key role in stabilizing the nucleotide. The aromatic ring of F179 was

dx.doi.org/10.1021/bi400170f | *Biochemistry* 2013, 52, 3543–3551

seen to lie parallel to the guanine ring in all the structures examined, implying the possibility of stable $\pi-\pi$ stacking (Figure 5). The time evolution of the dihedral angle, χ_2 (Cα−Cβ−Cγ−CD2), of F179 is shown in Figure S3 of the Supporting Information. It is clear that the conformation of F179 is very much dependent on the nucleotide state. The presence of GTP or GDP stabilizes the F179 conformation, which is otherwise extremely mobile. In very good agreement with this finding, the recent mutagenesis data with the F179W mutation (F182 in *Escherichia coli* FtsZ) showed no GTPase activity or FtsZ assembly.[50]

The difference between GDP- and GTP-FtsZ arises primarily because of the γ-phosphate and the appearance of the Mg^{2+} ion in the nucleotide binding pocket of GTP-FtsZ. The γ-phosphate oxygens form hydrogen bonds with peptide bond nitrogens of Ala67 and Ala69 in 55.17 and 59.17% of the total samples, respectively. The Mg^{2+} ion is found to be hexacoordinated, with the coordination shell consisting of γ-phosphate, β-phosphate, and four adjacent water molecules. These additional interactions impart greater stability to the nucleotide in the Z^T state, as shown in Figure 5. Because of this local interaction network in the nucleotide binding pocket of GTP-FtsZ, the phosphate clamp becomes very rigid (Figure S4 of the Supporting Information), which imparts a torsional flip to the guanine moiety of GTP. The flipping of the guanine moiety pulls along the top portion of core helix H7 and thus produces a compact H7−guanine−H1 sandwich (as exemplified by a narrow angle distribution in Figure 4b). Interestingly, one of the four water molecules that coordinated the Mg^{2+} ion was located 3.0−3.8 Å from Pγ with an angle of >110° with respect to the Pγ−O3β axis (Figure 5 and Figure S5 of the Supporting Information), thus fulfilling the conditions of the active water conformation for GTP hydrolysis.[51]

Essential Motions of FtsZ in Z^D, Z^T, and Z^0 States. Our findings suggest that nucleotides can impart local effects on the flexibility of FtsZ. However, because of the high dimensionality of the protein, it was rather difficult to identify the motions that are of biological importance. Hence, we performed PCA to locate the essential motions of FtsZ in each simulation ensemble. Figure 6a shows the relative contributions of different modes (eigenvectors) to the overall motion of the protein. The figure clearly shows that the bulk of the protein dynamics can be described by a small number of eigenvectors, which represent collective motions of atoms. The first 10 eigenvectors can describe ∼75% of the total mean-square fluctuation in the Z^D state, ∼70% in the Z^T state, and ∼85% in the Z^0 state. The inset shows that the first eigenvector contributes significantly, representing ∼35% of the total fluctuations in the Z^D state, ∼22% in the Z^T state, and ∼38% in the Z^0 state. To compare regions sampled by the essential motions in different nucleotide states, two-dimensional projections of MD ensembles onto the plane defined by the first two eigenvectors were plotted (Figure 6b−d). Notable differences in fluctuation were observed among the three states of FtsZ along eigenvectors 1 and 2. Although a considerable overlap in the cluster of conformations was observed, the dynamics of the Z^T state appears to be more restricted than those of the other two states.

The eigenvectors can be better interpreted by visualizing them through porcupine plots. To visualize an eigenvector, a cone is drawn for each residue starting from the Cα atom and projecting in the direction of the component of the same eigenvector that corresponds to that residue. The length of the cone represents the magnitude of the motion. Figure 7 shows the principal motions of FtsZ in three states, along the direction

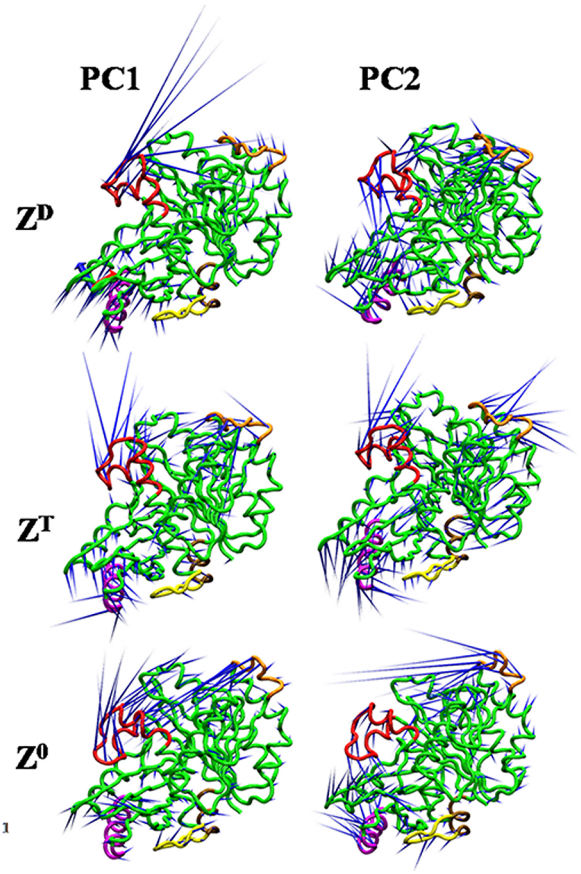

Figure 7. Porcupine plots representing the principal motions of FtsZ in Z^D, Z^T, and Z^0 states along the directions of PC1 and PC2. Secondary structural elements that underwent the most significant changes are highlighted: loops H6−H7 (red) and T3 (orange) in the N-domain and loop T7 (yellow) and helices H8 (brown) and H10 (magenta) in the C-domain. The structures of the protein are projected from the same angle in all states, resembling the orientation of FtsZ seen in the crystal structure of a semicontinuous protofilament.[22]

of principal components 1 and 2 (PC1 and PC2, respectively). The protein residues that are known to be involved in filament formation, such as helix H7 and loop T3 in the N-domain and helices H8−H10 and loop T7 in the C-domain, show the largest average velocity covariance vectors. Moreover, remarkable concerted motions are seen between the H6−H7 region and loop T3 in the N-domain and helices H9 and H10 and loop T7 in the C-domain. Another noteworthy feature is that both PC1 and PC2 showed significant differences in the direction of residue displacements, particularly in the H6−H7 region and loop T3 in the three states. While the displacements of the H6−H7 region are approximately along the radial direction in Z^D and Z^0 states, they were directed longitudinally in the Z^T state. Similarly, the vectors of loop T3 in the Z^T state are directed more longitudinally than those of the other two states. Also, in this state, helices H8−H10, which reside opposite the H6−H7 and T3 loop region, show prominent longitudinal movement in the opposite direction (in PC1 and PC2). Recall that the H6−H7 region makes contacts with helix H10 during FtsZ filament formation.[22] Taken together, the

dx.doi.org/10.1021/bi400170f | *Biochemistry* 2013, 52, 3543−3551

results suggest that GTP can increase the likelihood of FtsZ assembly by subtly modifying the surface residues and by inducing concerted motions in N- and C-domains, which are complementary to each other. The observed concerted motion is consistent with the site-directed mutagenesis data, where one damaged interface surface of the FtsZ subunit was found to induce a much weaker interaction with the other surface for polymer elongation.[52] Also, the larger covariance vectors of the H6−H7 region in the Z^D state are consistent with its high local fluctuations, as seen from rmsf calculations in Figure 3. In Figure 7, the structures of FtsZ are projected from the same angle as in the crystal structure of MjFtsZ in a semicontinuous nucleotide-free protofilament.[22]

DISCUSSION

We employ MD simulations and ED analysis to investigate the effects of nucleotide states on the structure and dynamics of monomeric FtsZ. Three independent simulations were performed on GDP-bound, GTP-bound, and nucleotide-free monomeric FtsZ. Results indicate that GDP-bound FtsZ and GTP-bound FtsZ are not very structurally different (Figure 2). However, they differ substantially in their dynamics. In all three states, the H6−H7 region, composed of helix H6, loop H6−H7, and the top portion of core helix H7, shows significant flexibility (Figure 3). This region deviates up to 6.5 Å in the GDP simulation, 13 Å in the nucleotide-free simulation, and 4 Å in the GTP simulation from the average structure. The differential flexibility between GDP- and GTP-bound FtsZ arises mainly due to the GTP γ-phosphate and Mg^{2+} ion that reside in the nucleotide binding pocket of GTP-FtsZ. The γ-phosphate oxygens stabilize the protein residues locally by interacting with the T3 loop region. The hexacoordinated Mg^{2+} ion with its coordinating elements (γ-phosphate, β-phosphate, and four adjacent water molecules) provides additional stability to GTP-bound FtsZ. Because of this interaction network in the nucleotide binding pocket, the phosphate clamp of GTP becomes very rigid, which imparts a torsional flip to the nucleotide guanine moiety. The flipping of the guanine moiety pulls along the top portion of core helix H7 and produces a compact H7−guanine−H1 sandwich (Figure 5b). In GTP-bound FtsZ, therefore, the H7−H1 angle is smaller and the protein samples the less curved conformations (around the nucleotide binding region) more often than the GDP-bound or nucleotide-free state (Figure 4b). In nucleotide-free state, the absence of a nucleotide imparted a twisted bending to helix H7 and slight rotation to the C-domain, which have opened the nucleotide binding cleft for the protein to sample the widely curved conformations predominantly (around the nucleotide binding region). These results thus suggest that the H6−H7 region can act as a switch element, which can modulate the FtsZ conformation by recognizing the nucleotide state. The switching of the H6−H7 region is possible, because neither helix H6, loop H6−H7, nor the top portion of helix H7 is trapped in the rigid subdomains of FtsZ or stabilized solely by the nucleotide. The observed conformational flexibility in FtsZ is consistent with mutagenesis data of Chen and Erickson,[50] where the tryptophan mutant, L189W, located on helix H7 and buried between the N- and C-terminal domains in *E. coli* FtsZ showed a large fluorescence increase, indicating a shift or rotation of the two domains upon assembly. The importance of domain movements was further tested by an S154C/Y222C double-cysteine mutant, which blocked FtsZ activity by disulfide lock in *E. coli*. This implies that the conformational flexibility in the FtsZ subunit is as important as the interfaces for assembly.

To probe if the H6−H7 region can act as a switch element, we performed principal component analysis on the simulation trajectories. The analysis strengthened our finding by showing the largest average velocity covariance vectors for the H6−H7 region (Figure 7). This analysis also shows remarkable concerted motions between the H6−H7 region and other functionally important elements of the protein, such as loop T3 in the N-domain and helices H9 and H10 and loop T7 in the C-domain. Moreover, in GTP-bound FtsZ, the directions of residue displacements are found to be more longitudinal than in the other two states. In the GDP-bound and nucleotide-free states, the movements of the H6−H7 region and other regions are largely random (compare the directions of the vectors in PC1 and PC2 of a given state). Also, the directions of the longitudinal movements of the H6−H7 region and loop T3 in GTP-FtsZ are the opposite of the directions of the movements of helix H10 and loop T7 (upward vs downward vectors). Recall that during filament formation the N-domain of the lower subunit contacts the C-domain from the upper subunit. These longitudinal movements of the structural elements of GTP-FtsZ are likely to facilitate the assembly of FtsZ into straight filaments. On the contrary, the radial or random movements of FtsZ residues may not allow the GDP-bound monomers to assemble as efficiently as GTP-FtsZ monomers and could produce curved filaments.[3] The superposition of the simulated structures onto the MjFtsZ crystal structure in semicontinuous filaments reconfirms our conclusions, showing the dominant movements of functionally relevant elements along the upper FtsZ subunit for effective binding in the GTP state (Figure S6 of the Supporting Information). The results are in very good agreement with *in vitro* studies and recent simulation results, where GTP-FtsZ filaments were found to be straight or gently curved while filaments of GDP-FtsZ were strongly curved.[23,49,54,55] The involvement of H7, H6−H7, H8, H10, T7, etc., in the assembly process is also in consistent with mutagenesis data, where mutations of the key amino acids at these secondary elements in the monomer−monomer interface (e.g., $N186K_{H7}$, $F182C/D_{H7}$, $F210A_{H8}$, $D273K_{H10}$, $N207C_{T7}$, $F182W_{H7}$, $L199W_{H7}$, $D209A_{H7}$, $D212A_{H7}$, $G211V_{H7}$, and $K228A_{T7}$ in *E. coli* FtsZ[48,50,52,53]) led to either deviated polymer assembly and disassembly or complete loss of division function. Thus, a detailed understanding of the differential competence of GTP- and GDP-FtsZ in polymer stability emerged from this study. These insights could be helpful in future drug design strategies, involving the development of nucleotide mimetics or small molecules that can selectively inhibit FtsZ assembly.

ASSOCIATED CONTENT

Supporting Information

Nucleotide-dependent conformational flexibility of FtsZ (Figures S1−S3), mobility of the phosphate clamp (Figure S4), location of the active water (Figure S5), and simulated FtsZ structures projected on the MjFtsZ crystal structure in a semicontinuous filament (Figure S6) as described in the text. This material is available free of charge via the Internet at http://pubs.acs.org.

AUTHOR INFORMATION

Corresponding Author

*Phone: +91-44-2257-4122. Fax: +91-44-2257-4102. E-mail: sanjibs@iitm.ac.in.

Funding

This work was supported by the Department of Biotechnology (DBT), Government of India. K.N. acknowledges the Council of Scientific and Industrial Research (CSIR), India, for the research fellowship.

Notes

The authors declare no competing financial interest.

ACKNOWLEDGMENTS

The computer resources of Computer Centre, IIT Madras, are gratefully acknowledged.

REFERENCES

(1) Lowe, J., and Amos, L. A. (1998) Crystal structure of the bacterial cell-division protein FtsZ. *Nature 391*, 203−206.

(2) Margolin, M. (2005) FtsZ and the division of prokaryotic cells and organelles. *Nat. Rev. Mol. Cell Biol. 6*, 862−871.

(3) Romberg, L., and Levin, P. A. (2003) Assembly dynamics of the bacterial cell division protein FtsZ: Poised at the edge of stability. *Annu. Rev. Microbiol. 57*, 125−154.

(4) Fu, G., Huang, T., Buss, J., Coltharp, C., Hensel, Z., and Xiao, J. (2010) *In vivo* structure of the *E. coli* FtsZ-ring revealed by photoactivated localization microscopy (PALM). *PLoS One 5*, e12680.

(5) Schaffner-Barbero, C., Martín-Fontecha, M., Chacón, P., and Andreu, J. M. (2012) Targeting the assembly of bacterial cell division protein FtsZ with small molecules. *Chem. Biol. 7*, 269−277.

(6) Huang, Q., Tonge, P. J., Slayden, R. A., Kirikae, J., and Ojima, I. (2007) FtsZ: A novel target for tuberculosis drug discovery. *Curr. Top. Med. Chem. 7*, 527−543.

(7) Lock, R. L., and Harry, E. J. (2008) Cell-division inhibitors: New insights for future antibiotics. *Nat. Rev. Drug Discovery 7*, 324−338.

(8) Kapoor, S., and Panda, D. (2009) Targeting FtsZ for antibacterial therapy: A promising avenue. *Expert Opin. Ther. Targets 13*, 1037−1051.

(9) Haydon, D. J., Stokes, N. R., Ure, R., Galbraith, G., Bennett, J. M., et al. (2008) An inhibitor of FtsZ with potent and selective anti-staphylococcal activity. *Science 321*, 1673−1675.

(10) Elsen, N. L., Lu, L., Parthasarathy, G., Reid, J. C., Sharma, S., et al. (2012) Mechanism of cell division inhibitor PC190723: Modulation of FtsZ assembly and cooperativity. *J. Am. Chem. Soc. 134*, 12342−12345.

(11) Andreu, J. M., Schaffner-Barbero, C., Huecas, S., Alonso, D., Lopez-Rodriguez, M. L., et al. (2010) The antibacterial cell division inhibitor PC190723 is a FtsZ polymer stabilizing agent which induces filament assembly and condensation. *J. Biol. Chem. 285*, 14239−14246.

(12) Lppchen, T., Hartog, A. F., Pinas, V. A., Koomen, G. J., and den Blaauwen, T. (2005) GTP analogue inhibits polymerization and GTPase activity of the bacterial protein FtsZ without affecting its eukaryotic homologue tubulin. *Biochemistry 44*, 7879−7884.

(13) Lppchen, T., Pinas, V. A., Hartog, A. F., Koomen, G. J., Schaffner-Barbero, C., et al. (2008) Probing FtsZ and tubulin with C8-substituted GTP analogs reveals differences in their nucleotide binding sites. *Chem. Biol. 15*, 189−199.

(14) Schaffner-Barbero, C., Gil-Redondo, R., Ruiz-Avila, L. B., Huecas, S., Läppchen, T., den Blaauwen, T., Diaz, J. F., Morreale, A., and Andreu, J. M. (2010) Insights into nucleotide recognition by cell division protein FtsZ from a *mant*-GTP competition assay and molecular dynamics. *Biochemistry 49*, 10458−10472.

(15) Margalit, D. N., Romberg, L., Mets, R. B., Hebert, A. M., Mitchison, T. J., Kirschner, M. W., and RayChaudhuri, D. (2004) Targeting cell division: small-molecule inhibitors of FtsZ GTPase perturb cytokinetic ring assembly and induce bacterial lethality. *Proc. Natl. Acad. Sci. U.S.A. 101*, 11821−11826.

(16) Park, Y. S., Grove, C. I., Gonzalez-Lopez, M., Urgaonkar, S., Fettinger, J. C., and Shaw, J. T. (2011) Synthesis of (−)-viriditoxin: A 6,6′-binaphthopyran-2-one that targets the bacterial cell division protein FtsZ. *Angew. Chem., Int. Ed. 50*, 3730−3733.

(17) Plaza, A., Keffer, J. L., Bifulco, G., Lloyd, J. R., and Bewley, C. A. (2010) Chrysophaentins A-H, antibacterial bisdiarylbutene macrocycles that inhibit the bacterial cell division protein FtsZ. *J. Am. Chem. Soc. 132*, 9069−9077.

(18) Haydon, D. J., Bennett, J. M., Brown, D., Collins, I., Galbraith, G., Lancett, P., Macdonald, R., Stokes, N. R., Chauhan, P. K., Sutariya, J. K., Nayal, N., Srivastava, A., Beanland, J., Hall, R., Henstock, V., Noula, C., Rockley, C., and Czaplewski, L. (2010) Creating an antibacterial with *in vivo* efficacy: Synthesis and characterization of potent inhibitors of the bacterial cell division protein FtsZ with improved pharmaceutical properties. *J. Med. Chem. 53*, 3927−3936.

(19) Kumar, K., Awasthi, D., Lee, S., Zanardi, I., Ruzsicska, B., Knudson, S., Tonge, P. J., Slayden, R. A., and Ojima, I. (2011) Novel trisubstitued benzimidazoles, targeting Mtb FtsZ, as a new class of antitubercular agents. *J. Med. Chem. 54*, 374−381.

(20) Beuria, T. K., Santra, M. K., and Panda, D. (2005) Sanguinarine blocks cytokinesis by inhibiting FtsZ assembly and bundling. *Biochemistry 44*, 16584−16593.

(21) Huecas, S., Schaffner-Barbero, C., Garcia, W., Yebenes, H., Palacios, J., et al. (2007) The interactions of cell divison protein FtsZ with guanine nucleotides. *J. Biol. Chem. 282*, 37515−37528.

(22) Oliva, M. A., Cordell, S. C., and Löwe, J. (2004) Structural insights into FtsZ protofilament formation. *Nat. Struct. Mol. Biol. 11*, 1243−1250.

(23) Huecas, S., and Andreu, J. M. (2004) Polymerization of nucleotide-free, GDP- and GTP-bound cell division protein FtsZ: GDP makes the difference. *FEBS Lett. 569*, 43−48.

(24) Oliva, M., Trambaiolo, D., and Lowe, J. (2007) Structural insights into the conformational variability of FtsZ. *J. Mol. Biol. 373*, 1229−1242.

(25) Li, Z., Trimble, M. J., Brun, Y. V., and Jensen, G. J. (2007) The structure of FtsZ filaments in vivo suggests a force-generating role in cell divison. *EMBO J. 26*, 4694−4708.

(26) Osawa, M., Anderson, D. E., and Erickson, H. P. (2008) Reconstitution of contractile FtsZ rings in liposomes. *Science 320*, 792−794.

(27) Osawa, M., Anderson, D. E., and Erickson, H. P. (2009) Curved FtsZ protofilaments generate bending forces on liposome membranes. *EMBO J. 28*, 3476−3484.

(28) Osawa, M., and Erickson, H. P. (2011) Inside-out Z rings: Constriction with and without GTP hydrolysis. *Mol. Microbiol. 81*, 571−579.

(29) Surovtsev, I. V., Morgan, J. J., and Lindahl, P. A. (2008) Kinetic modeling of the assembly, dynamic steady state, and contraction of the FtsZ ring in prokaryotic cytokinesis. *PLoS Comput. Biol. 4*, e1000102.

(30) Lan, G. H., Daniels, B. R., Dobrowsky, T. M., Wirtz, D., and Sun, S. X. (2009) Condensation of FtsZ filaments can drive bacterial cell division. *Proc. Natl. Acad. Sci. U.S.A. 106*, 121−126.

(31) Allard, J. F., and Cytrynbaum, E. N. (2009) Force generation by a dynamic Z-ring in *Escherichia coli* cell division. *Proc. Natl. Acad. Sci. U.S.A. 106*, 145−150.

(32) Erickson, H. P. (2009) Modeling the physics of FtsZ assembly and force generation. *Proc. Natl. Acad. Sci. U.S.A. 106*, 9238−9243.

(33) Natarajan, K., Mohan, J., and Senapati, S. (2013) Relating nucleotide dependent conformational changes in free tubulin dimer to tubulin assembly. *Biopolymers 99*, 282−291.

(34) Natarajan, K., and Senapati, S. (2012) Understanding the basis of drug resistance of the mutants of $\alpha\beta$-tubulin dimer *via* molecular dynamics simulations. *PLoS One 7* (8), e42351.

(35) Case, D. A., Darden, T. A., Cheatham, T. E., Simmerling, C. L., Wang, J., et al. (2010) *Amber*, version 11, University of California, San Francisco.

(36) Vriend, G. (1990) WHAT IF: A molecular modeling and drug design program. *J. Mol. Graphics 8*, 52−56.
(37) Frisch, M. J., Trucks, G. W., Schlegel, H. B., Scuseria, G. E., Robb, M. A., et al. (2009) *Gaussian 09*, revision A.1, Gaussian Inc., Wallingford, CT.
(38) Cornell, W. D., Cieplak, P., Bayly, C. I., and Kollmann, P. A. (1993) Application of RESP charges to calculate conformational energies, hydrogen bond energies, and free energies of solvation. *J. Am. Chem. Soc. 115*, 9620−9631.
(39) Jorgensen, W. L., Chandrasekhar, J., Madura, J. D., Impey, R. W., and Klein, M. L. (1983) Comparison of simple potential functions for simulating liquid water. *J. Chem. Phys. 79*, 926−935.
(40) Essmann, U., Perera, L., Berkowitz, M. L., Darden, T., Lee, H., et al. (1995) A smooth particle mesh Ewald method. *J. Chem. Phys. 103*, 8577−8593.
(41) Ryckaert, J. P., Ciccotti, G., and Berendsen, H. J. C. (1977) Numerical integration of the cartesian equations of motion of a system with constraints: Molecular dynamics of n-alkanes. *J. Comput. Phys. 23*, 327−341.
(42) Phillips, J. C., Braun, R., Wang, W., Gumbart, J., Tajkhorshid, E., et al. (2005) Scalable molecular dynamics with NAMD. *J. Comput. Chem. 26*, 1781−1802.
(43) Hornak, V., Abel, R., Okur, A., Strockbine, B., Roitberg, A., et al. (2006) Comparison of multiple amber force fields and development of improved protein backbone parameters. *Proteins 65*, 712−725.
(44) Berendson, H. J. C., and Hayward, S. (2000) Collective protein dynamics in relation to function. *Curr. Opin. Struct. Biol. 10*, 165−169.
(45) Berendsen, H. J. C., Van Der Spoel, D., and Van Drunen, R. (1995) GROMACS: A message-passing parallel molecular dynamics implementation. *Comput. Phys. Commun. 91*, 43−56.
(46) Barrett, C. P., and Noble, N. E. M. (2004) Dynamite: A simple way to gain insight into protein motions. *Acta Crystallogr. 60*, 2280−2287.
(47) Humphrey, W., Dalke, A., and Schulten, K. (1996) VMD: Visual Molecular Dynamics. *J. Mol. Graphics 14*, 33−38.
(48) Martín-Galiano, A. J., Buey, R. M., Cabezas, M., and Andreu, J. M. (2010) Mapping flexibility and the assembly switch of cell division protein FtsZ by computational and mutational approaches. *J. Biol. Chem. 285*, 22554−22565.
(49) Hsin, J., Gopinathan, A., and Huang, K. C. (2012) Nucleotide-dependent conformations of FtsZ dimmers and force generation observed through molecular dynamics simulations. *Proc. Natl. Acad. Sci. U.S.A. 109*, 9432−9437.
(50) Chen, Y., and Erickson, H. P. (2011) Conformational changes of FtsZ reported by tryptophan mutants. *Biochemistry 50*, 4675−4684.
(51) Martin-Garcia, F., Salvarelli, E., Mendieta-Moreno, J. I., Vincente, M., Mingorance, J., et al. (2012) Molecular dynamics simulation of GTPase activity in polymers of the cell division protein FtsZ. *FEBS Lett. 586*, 1236−1239.
(52) Redick, S. D., Stricker, J., Briscoe, G., and Erickson, H. P. (2005) Mutants of FtsZ targeting protofilament interface: Effects on cell division and GTPase activity. *J. Bacteriol. 187*, 2727−2736.
(53) Stricker, J., and Erickson, H. P. (2003) In vivo characterization of *Escherichia coli* FtsZ mutants: Effects on Z-ring structure and function. *J. Bacteriol. 185*, 4796−4805.
(54) Lu, C., Reedy, M., and Erickson, H. P. (2000) Straight and curved conformations of FtsZ are regulated by GTP hydrolysis. *J. Bacteriol. 182*, 164−170.
(55) Erickson, H. P., Taylor, D. W., Taylor, K. A., and Bramhill, D. (1996) Bacterial cell division protein FtsZ assembles into protofilament sheets and minirings, structural homologs of tubulin polymers. *Proc. Natl. Acad. Sci. U.S.A. 93*, 519−523.